Jun-Yi Ge, Vladimir N. Gladilin, Joffre Gutierrez, and
Victor V. Moshchalkov

5 Direct visualization of vortex patterns in superconductors with competing vortex-vortex interactions

Abstract: In superconductors, the interaction between vortices as a function of the distance between them can be either monotonic or nonmonotonic mainly due to the special characteristic parameter lengths, i.e., the penetration depth and coherence length. In traditional type-II superconductors with purely repulsive vortex-vortex interactions, a triangular vortex lattice is formed, which is also known as the Abrikosov vortex lattice. In superconductors with competing vortex-vortex interactions, such as type-I, low-κ and type-1.5 superconductors, much more complex vortex patterns can be formed. Because of the analogy to other systems with modulated phases, the study of vortex matter has attracted a lot of interest. In this chapter, we present recent progress in this field concerning direct visualization of these vortex patterns with scanning Hall probe microscopy.

5.1 Introduction

Interaction is explained as a kind of action that occurs as two or more objects have an effect upon one another. While in some cases the interaction is simply monotonic, i.e., purely "repulsive" or "attractive", in most cases its nature is a combination of several complex contributions which can even be competing. The latter widely exists in nature and strongly affects the main characteristics of many systems.

In natural sciences, many systems have been found to exhibit complex interactions among different phases. To name a few [1], we mention the ferrofluid system, reaction-diffusion in chemical mixtures, convection of a fluid with a temperature gradient and superconducting systems. All these systems present various modulated patterns due to complex interactions. The study of these systems, especially at the microscopic level, can give us a lot of information about the relevant mechanisms. It can also help us to better understand the macroscopic properties which, in the future, can result in different applications. Among all these systems, the superconducting system is an ideal candidate since different kinds of superconductors show different complex vortex patterns. In type-II superconductors, the Abrikosov vortex lattice with triangular arrangement of vortices forms due to the purely repulsive interaction between

Jun-Yi Ge, Vladimir N. Gladilin, Joffre Gutierrez, Victor V. Moshchalkov, KU Leuven, Celestijnenlaan 200D, B-3001 Leuven, Belgium email: Victor.Moshchalkov@fys.kuleuven.be

DOI 10.1515/9783110456806-006,

them, while in type-I superconductors, vortex interaction becomes long-range repulsive and short-range attractive, thus leading to the formation of the intermediate state. The interactions between vortices can also be long-range attractive and short-range repulsive as revealed in low-κ superconductors [2] and the recently discovered type-1.5 superconductors [3, 4], both of which display intricate vortex patterns with coexistence of a large Meissner area, vortex stripes and clusters.

Compared with other systems, it is quite convenient to manipulate the parameters related to the vortex interaction in superconductors, like the magnetic field and temperature. One can also introduce other interactions to the system, e.g., by adding artificially fabricated pinning centers [5], amplifying confinement effects in mesoscopic- and nanosuperconductors [6], combining two superconducting condensates with different characteristic lengths (λ, penetration depth; ξ, coherence length) in bilayer structures [7], and so on.

Motivated by the recent progress, in this chapter we present the scanning Hall probe microscopy (SHPM) results for the intricate vortex patterns and related phenomena in a few selected superconducting systems with different competing vortex-vortex (v–v) interactions.

The chapter is organized as follows. In Section 5.2, we introduce the background to the classification of superconductors. Section 5.3 describes the experimental framework used to visualize the vortex patterns in different types of superconductors. Sections 5.4 and 5.5 present the experimental results on vortex patterns as well as their dynamical behaviors. Finally, Section 5.6 presents the conclusions.

5.2 Classification of superconductors

5.2.1 Single-component superconductors

Superconductivity is a thermodynamic equilibrium phase, indicating that the electron gas condensed in a novel macroscopic quantum state below the critical temperature T_c has a lower free energy than the electron gas in a normal metal. When a superconductor is placed in a magnetic field, the exclusion of the magnetic field will increase its free energy. This means that the Meissner effect can only survive a finite applied magnetic field, since the increase of free energy with increasing magnetic field will compensate for the drop in free energy associated with condensation of the electron gas. At the thermodynamic field H_c the two effects balance each other, while above H_c a transition from superconductivity to the normal state will occur. It has been found that the reaction of superconductors to the presence of a magnetic field strongly depends on material properties, i.e., the characteristic lengths. Regardless of the sample shape, some superconductors exhibit only partial flux expulsion while others show full Meissner state. To study the difference, we need to consider the energy cost per unit interfacial area when a superconductor/normal interface is formed. This energy

cost has the order of [8]:

$$\Delta G \sim \frac{\mu_0}{2}\left(\xi H_c^2 - \lambda H_a^2\right) \tag{5.1}$$

where H_a is the applied magnetic field. This energy determines different thermodynamic equilibrium states, leading to the classification of various superconductors. Detailed calculations based on the Ginzburg–Landau (GL) equations show that the critical value of $\kappa = \lambda/\xi$ that separates different superconductors is $1/\sqrt{2}$. For type-I superconductors with $\kappa < 1/\sqrt{2}$, the interface energy is positive, while for type-II superconductors with $\kappa > 1/\sqrt{2}$, it becomes negative. However, the equations are based on Landau's second-order phase transition theory. Strictly speaking, it only works fine at T_c. While well below T_c, corrections must be introduced. In the 1960s, it was found that the corrections modify the interaction potential at large distances which leads to a new kind of superconductor, called type-II/1, that exists in a very narrow κ range. In order to distinguish from type-II/1, the traditional type-II superconductor is called type-II/2.

Each kind of superconductor exhibits a characteristic behavior in the presence of a magnetic field. For a type-I superconductor, the Meissner state is observed up to H_c since the energy cost of letting the magnetic field penetrate the superconductor is positive. Above H_c, the normal state is restored for the whole material. Figure 5.1a presents the typical $M(H)$ (magnetization versus field) curve for a type-I superconductor without a demagnetization effect (e.g., for an infinitely long cylinder with H parallel to the cylinder axis). However, in reality, any sample has a demagnetization effect, and the magnetic field at the edges of the sample is enhanced by a factor of $H_a/(1-N)$, where N is the demagnetization factor. As a result, the magnetic field can penetrate from these areas even when the external field is smaller than H_c. Therefore, an interme-

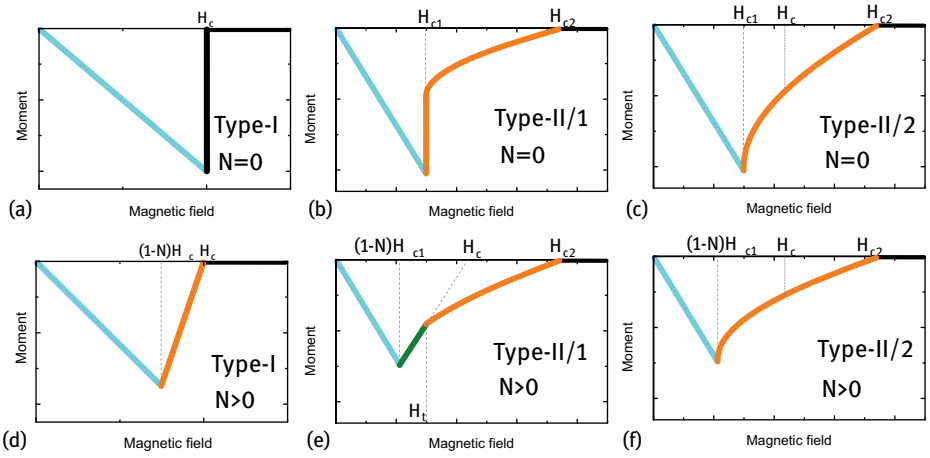

Fig. 5.1: (a)–(c) Representative M(H) curves for type-I, type-II/1 and type-II/2 superconductors without (a)–(c) and with (d)–(f) a demagnetization effect.

diate state with coexistence of superconducting regions and normal states is formed. The typical magnetization curve is shown in Figure 5.1d. In type-I superconductors, two contributions to the v-v interaction are present: 1) the attractive interaction arising from positive interface energy; 2) the repulsive magnetic interaction between the stray field of normal domains. This competition between the vortex interactions leads to the formation of an intermediate state with flux tubes, stripes and so on.

For type-II/2 superconductors with $\xi \ll \lambda$, the Meissner state can only be maintained below a lower critical field H_{c1}, above which the superconducting/normal interface energy becomes negative, and the magnetic field will penetrate the sample in the form of single quantum vortices (to maximize the S/N interface area), forming what is called a mixed state (MS). With a further increase of the field, the normal state will be restored at an upper critical field H_{c2}, if we are to ignore the surface (or H_{c3}) superconductivity effect. The v-v interaction in type-II superconductor is purely repulsive. This means that, for a given flux density, vortices will try to maximize the distance between each other, leading to the formation of a triangular lattice, also known as the Abrikosov vortex lattice. The typical magnetization curves for a type-II superconductor with and without a demagnetization effect are shown in Figure 5.1c and f, respectively.

With κ in a narrow range close to $1/\sqrt{2}$, type-II/1 superconductors exhibit both type-I and type-II behaviors on the magnetization curve [2, 9–12]. As shown by Figure 5.1b, the superconductor experiences a first-order transition at H_{c1} from the Meissner state to a mixed state and then progressively transits to the normal state at H_{c2}. Accompanying the first-order transition, a magnetization jump is clearly observed at H_{c1}. The flux patterns for low-κ superconductors with a demagnetization factor N were also studied by the Bitter decoration technique. It was found that in the field range $(1-N)H_{c1} < H_a < H_t$, clusters with triangular vortex lattices coexist with Meissner areas. This new state is now known as the intermediate mixed state (IMS). With further increasing of the field up to H_t all Meissner areas are filled with triangular vortex lattices that behave like a traditional type-II superconductor (Figure 5.1e). The formation of IMS is due to the long-range attractive and short-range repulsive v-v interaction. The first theoretical study of an attractive vortex interaction was done by Eilenberger and Buttner [13]. They solved rigorously the Gorkov equations for the vortex by asymptotic expansions for large values of distance r, and obtained oscillations in the magnetic field distributions at low temperatures when κ was decreased below a critical value 1.7, which might result in an attractive interaction between vortices. Later, a similar field reversal was also observed by Dichtel [14] and Halbritter [15] from a nonlocal approximation. However, Leung and Jacobs [16, 17] have shown that the oscillatory behavior of the vector potential disappears when considering a term related to the surface barrier which was neglected in the last mentioned works. Finally, the vortex attractions were analyzed in detail from Eilenberger's reformulation of the Gorkov equations, and Jacobs and Hubert concluded that microscopic corrections can indeed lead to vortex attraction at long distances in low κ superconductors [16, 17].

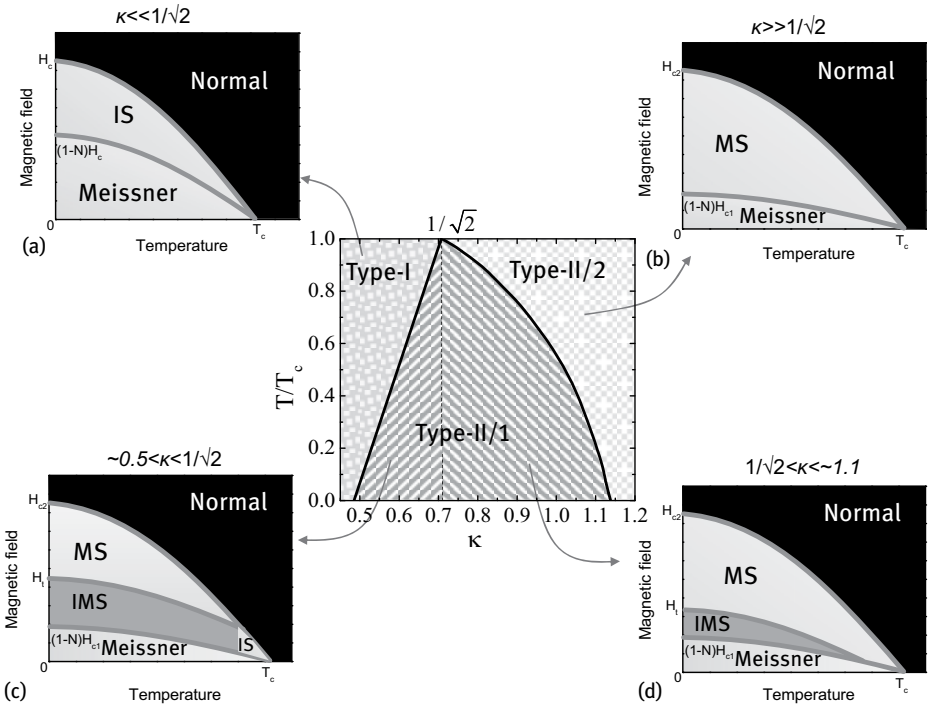

Fig. 5.2: κ–T phase diagram for different kinds of single component (single gap) superconductors with the demagnetization factor of N. (a)–(d) MT phase diagram for superconductors with various κ indicated.

In Figure 5.2 we summarized the MT phase diagram for the above-mentioned superconductors with various κ.

5.2.2 Type-1.5 superconductors

The three types of superconductors introduced in Section 5.2.1 are all based on one component (single gap) superconductors. In superconductors with two or more gaps, the interactions between vortices and the appropriate theory to describe them becomes even more complex. In 2005, Babaev et al. proposed the "*semi-Meissner state*" in multiband superconductors where each condensate has its characteristic coherence length, $\xi_1, \xi_2 \ldots$ [3]. When some of them are larger and the rest are smaller than the penetration depth, e.g., $\xi_1/\sqrt{2} < \lambda < \xi_2/\sqrt{2}$ in a two-band superconductor, vortices can have long-range attractive (due to overlap of outer cores) and short-range repulsive interaction (current-current and electromagnetic interaction). As a result, these superconductors exhibit a first-order transition from the Meissner state into the semi-Meissner state, a mixture of the Meissner state and vortex clusters.

In 2009, Moshchalkov et al. found that the two characteristic lengths of the π and σ bands in MgB_2 material fulfill the requirement for the nucleation of a semi-Meissner state [4]. By using Bitter decoration they reported the observation of such a semi-Meissner state with a mixture of vortex clusters, stripes and large areas of Meissner state. For the first time, this new state was termed a type-1.5 superconductor. Later on, the disordered state was also observed by scanning Hall probe microscopy [18] and scanning SQUID microscopy measurements [19]. Recently, type-1.5 superconductivity was reported in another two-band superconductor Sr_2RuO_4 [20, 21]. Highly nontrivial vortex patterns, similar to type-1.5 superconductivity, have been predicted for a type-1/type-II bilayer system [22, 23]. Possible type-1.5 superconductivity is also suggested for other two-band and multiband superconductors, such as the large family of Fe-based superconductors [24–26] and $Lu_2Fe_3Si_5$ [27].

Although type-1.5 superconductivity has similar vortex interactions and phase diagrams to type-II/1 superconductors, the mechanisms behind them are quite different. Moreover, the GL parameter κ in type-1.5 superconductors can reach a value far away from the dual point $1/\sqrt{2}$, e.g., $\kappa \sim 5$ for MgB_2 [28].

Besides the situation in MgB_2, theorists suggest that the definition of type-1.5 superconductivity should be extended to more general cases. Babaev et al. reported that type-1.5 behavior can arise via the proximity effect between one superconducting and one normal band, even when this interband effect is very small [29]. Self-organization into stripe phases is also suggested in a two-dimensional assembly of particles with two isotropic repulsive interactions [30, 31]. This may also work for vortices in multiband superconductors with $\xi_{1,2\ldots}/\sqrt{2} < \lambda$. Indeed, experimental study on a dirty MgB_2 film, where the GL parameter for both bands is much bigger than $1/\sqrt{2}$, has shown very inhomogeneous distribution of vortices [32]. More experiments need to be done to further understand this effect.

5.3 Experimental

In this chapter, the vortex patterns are mainly imaged by using scanning Hall probe microscopy (SHPM). The working principle of the SHPM technique is based on the incorporation of a submicron-sized GaAs/AlGaAs heterostructure Hall sensor into a scanning probe technique [33]. The advantage of using a semiconductor heterostructure is that it has a very low carrier density. It is known that when a current-carrying conductor is placed in a perpendicular magnetic field, a transverse voltage V_H will appear due to the Lorentz force acting on the charge carriers. This effect is known as the Hall effect which was first discovered by the American physicist Edwin Herbert Hall in 1879 [34]. For a simple metal plate, V_H has the following expression:

$$V_H = -\frac{IB}{n_{3d}te} = -\frac{\mu IB}{\sigma t} \tag{5.2}$$

where I is the current flowing through the plate, B is the external magnetic field, n_{3d} is the carrier density, t is the plate thickness, e is the electron charge, μ is the carrier mobility and σ is the carrier conductivity. While scanning over a sample surface with magnetic modulation, the sensor picks up the perpendicular component of the local magnetic field $B_z(r)$ and produces a Hall voltage directly proportional to the field strength. In this way, a magnetic image of the sample can be mapped.

Besides mapping the magnetic field distribution, the SHPM has been modified to measure the local ac susceptibility of the superconductor under an ac magnetic field. This is implemented by separating the in-phase, V_1', and out-of-phase components, V_2' of V_H with a lock-in amplifier. These components are proportional to the in-phase and out-of-phase ac components of the local magnetic induction. This technique is named scanning ac-susceptibility microscopy (SacSM) with which we are able to study the vortex dynamics at the micrometer scale.

In summary, the major advantage of the SHPM technique is that it is noninvasive, which is important when the magnetic features of the sample should not be disturbed, like in the case of unpinned vortices in superconductors. Furthermore, it has a very high sensitivity, it gives fast, direct and quantitative information about the local magnetic field and the technique is applicable in externally applied magnetic fields and in a wide temperature range.

5.4 Type-I superconductor with long-range repulsive and short-range attractive v-v interaction

To study the flux patterns in type-I superconductors, a thick lead film with lateral dimensions of $1 \times 1\text{cm}^2$ and a thickness $d = 5\,\mu\text{m}$ is used. The sample was grown using an e-beam evaporation system. A 10 nm Ge layer was deposited on top to protect the Pb surface from oxidation. There is no obvious difference among the edges of the sample, therefore, the penetration of the flux is considered to be the same. The superconducting critical temperature is $T_c = 7.05$ K, as determined by the ac-susceptibility at zero applied magnetic field. All the experiments have been performed with the field applied perpendicular to the sample surface.

5.4.1 Flux patterns of the intermediate state

From the phase diagram in Figure 5.2, the intermediate state can be reached in two different ways, flux penetration and flux expulsion. The former is realized through sweeping up the magnetic field after the sample was cooled down ($T < T_c$) in zero magnetic field (ZFC; zero-field-cooled). The latter is done by imaging flux patterns when sweeping down the magnetic field, after the sample was field-cooled (FC) to a given fixed temperature close to $T_c(H)$.

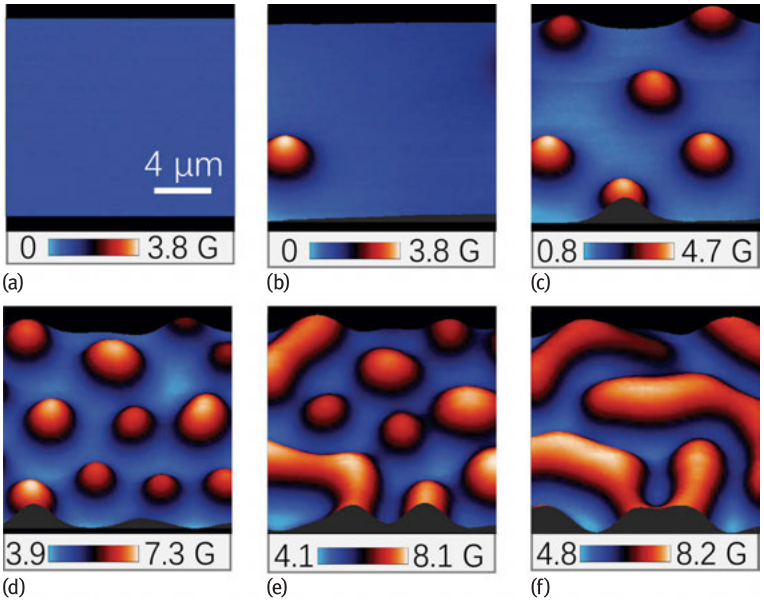

Fig. 5.3: Typical SHPM images of type-I Pb film obtained at different increasing magnetic fields after ZFC at 6.9 K: (a) 2 Oe, (b) 2.6 Oe, (c) 4.2 Oe, (d) 7.6 Oe, (e) 12 Oe, (f) 16 Oe. Blue and red areas correspond to superconducting and normal state, respectively.

Figure 5.3a–f shows the flux patterns of the intermediate state obtained with the SHPM during flux penetration at 6.9 K. At low fields, the sample is in the Meissner state with no flux observed in the scanning area (Figure 5.3a). When a certain magnetic field (≈ 2 Oe at 6.9 K) is reached, magnetic flux begins to penetrate the sample, forming flux tubes with a circular shape (Figure 5.3b). At first, the observed flux tubes have similar radii and vorticity as shown in Figure 5.3c; but with further increase of the field, the density of the flux tubes increases and they start to lose the circular shape, characteristic of lower densities. The tubes also exhibit a broader distribution of sizes and vorticities as shown in Figure 5.3d. When the magnetic field reaches a certain threshold (≈ 12 Oe at 6.9 K), the tubes are very close to each other, the N/S positive surface energy takes over and flux tubes start to merge to form stripe-like normal domains resulting in a state with coexistence of flux tubes and stripes (Figure 5.3e). As shown in Figure 5.3f, once it becomes favorable for the system to form stripes, they thrive as the magnetic field increases, resulting in the formation of longer stripes that eventually merge to form wider normal domains that cover the whole superconductor upon reaching $H_c(T)$ (≈ 25 Oe at 6.9 K).

Figure 5.4a–d shows the flux patterns of the intermediate state obtained with the SHPM during flux expulsion at 6.9 K. Figure 5.4a presents an SHPM image taken at 20 Oe and 6.9 K close to H_c, and normal regions surround small superconducting regions. As we decrease the magnetic field, in contrast to the case of flux penetration,

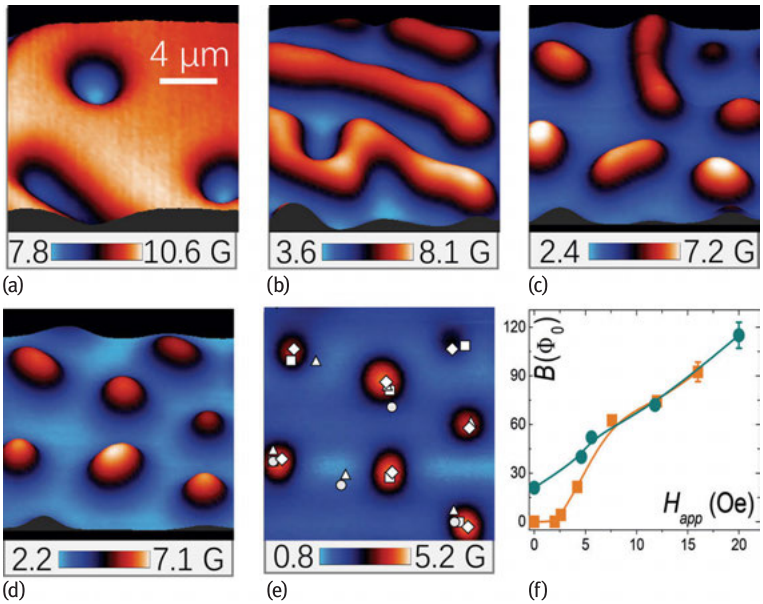

Fig. 5.4: SHPM images measured at 6.9 K after FC and then progressively decreased field from (a) 20 Oe to (b) 11.8 Oe, (c) 5.6 Oe, (d) 4.6 Oe and (e) remnant field. The symbols in (e) show the positions of flux tubes after various FC processes at $T = 6.9$ K and $H = 1.1$ Oe (circles); 1.9 Oe (triangles); 4.9 Oe (squares); 5.4 Oe (diamonds). Blue and red areas correspond to superconducting and normal state, respectively. (f) Local induction B as a function of the applied magnetic field H_{app} for images in Figure 5.3a–f (squares) and Figure 5.4 a–e (circles).

the stripe-like normal domains nucleate first (Figure 5.4b) and they last to significantly lower fields (Figure 5.4c), as compared to the flux penetration experiment (Figure 5.3e). As we keep on decreasing the magnetic field, part of the stripes breaks down into flux tubes until only flux tubes remain (Figure 5.4d). Finally, Figure 5.4e shows the flux pattern when the magnetic field has been decreased to zero, and it is worth noticing that, due to the pinning present in our sample, we do not recover the Meissner state.

Figure 5.4f shows the hysteresis in local induction B as a function of the applied magnetic field H_{app} for images in Figure 5.4a–f (squares) and Figure 5.4a–e (circles). It is clear that, for flux penetration, even at $62.5\Phi_0$ (Figure 5.3d), flux patterns remain in tubular state. However, for flux expulsion, the flux patterns change from stripe to tubular state for a magnetic flux value around $52\Phi_0$ (Figure 5.4c). In order to identify the most relevant pinning centers we performed at the same sample area a series of repeated FC processes at various fields and temperatures. We observed that each time the flux tubes nucleate around the same areas (we have labeled such areas in Figure 5.4e). Therefore, these positions should contain dominant pinning centers which could be produced by defects in the film formed during sample growth.

5.4.2 Topological hysteresis

As shown in the previous subsection, the flux patterns of the intermediate state mainly contain three topological states: 1) flux tubes; 2) flux stripes; 3) coexistence of flux tubes and stripes. By continuously imaging the flux patterns with SHPM at different temperatures and magnetic fields, the topological phase diagram of the flux patterns for the intermediate state can be constructed.

For the flux penetration process after ZFC, the intermediate state can be divided into three regions with different flux structures: Meissner state (no flux); Flux tube state; Stripe state. However, when accessing the flux expulsion process by performing field-cooling, the phase boundaries (dashed lines) are shifted to lower fields, and only flux stripe and flux tube states are observed. As follows from Figure 5.5, the so-called "topological hysteresis" exists in our sample [35], which has been reported previously for most of the type-I materials with the presence of pinning or geometrical barriers. In that regard, our sample is a thick film of type-I lead superconductor, therefore surface barriers and /or intrinsic pinning centers (arising due to sample growth conditions) should play an important role. We also mention that in a type-I superconductor without a geometric barrier, such as (hemi)spheres and cones, flux tubes dominate the intermediate field region [35]. The topological hysteresis is also found to be the origin of magnetic hysteresis in type-I superconductors. However, some questions still remain open for topological hysteresis. What is the dominating factor behind stripe structures? Why does such a large overlapped region for flux tubes and stripes exist?

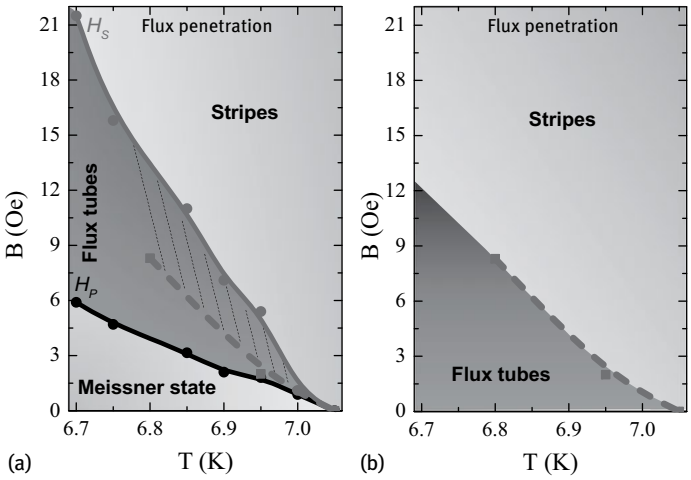

Fig. 5.5: Topological flux pattern phase diagram for flux penetration (a) and flux expulsion (b) of a type-I superconducting film. The green dashed line in (a) is the same phase boundary between flux stripes and flux tubes as seen in (b), showing topological hysteresis. The shaded area in (a) indicates a region where either flux tubes or stripes can form.

A theoretical estimate made by Goren and Tinkham showed that the tubular state and stripe state have approximately the same energy [36]. This means that the equilibrium superconducting state in an intermediate state can be easily affected by various factors such as the presence of pinning centers and differences in sample geometry. We will further introduce the dynamical behaviors and try to answer the above questions in Section 5.4.4.

5.4.3 Quantization of fluxoids in the intermediate state

Following the single-valuedness of the order parameter, the amount of flux over any closed path in a superconductor must be quantized, with flux quantum $\phi_0 = h/2e = 2.067\,\mathrm{mT\mu m^2}$. In type-II and type-1.5 superconductors each fluxoid contains one single flux quantum Φ_0, while in type-I superconductors the normal domains, since flux is quantized, contain multiple Φ_0. As shown in Section 5.4.1, all the flux patterns in the intermediate state are formed by individual or combined flux tubes. Therefore, flux tubes can be considered as the basic block for the formation of the intermediate state. It is of great fundamental interest and importance to answer the following questions: first, how do the flux tubes interact with each other? It is natural to expect that the interaction (merging or annihilating) between two flux tubes must also happen through quantized flux. However, it has never been confirmed experimentally. Theoretical results have revealed that the nucleation and interaction of flux domains under an applied current are both occurring via the nucleation of individual flux quanta [37].

Therefore, this gives rise to a second question, is it possible to have stable flux domains with a single flux quantum in the intermediate state of a type-I superconductor? In the 1960s, theoretical work had shown that, in thin-enough type-I superconductor films with perpendicular magnetic field, the transition from superconducting to normal state can be type-II like [38, 39], and a triangular vortex lattice may favor a more energetically stable state [40]. Various experimental results have also confirmed such a prediction [41, 42]. The critical thickness, d_c, below which single vortices can exist, varies with the material [43, 44] (e.g., $d_c \sim 200\,\mathrm{nm}$ for Pb; $\sim 110\,\mathrm{nm}$ for In). Very recently, the single flux quantum vortices have been suggested to exist in mesoscopic type-I materials with strong confinement effects [45]. Engbarth et al. reported the observation of Φ_0 vortices in a 1D type-I Pb nanowire through local magnetization measurements [46]. However, in macroscopic samples, Φ_0 fluxoids have never been observed neither experimentally nor reported theoretically. Is it possible to stabilize single-quantum vortices in the intermediate state of a macroscopic type-I superconductor? If not, what would be the minimum possible flux for the intermediate state? It is believed that, due to the connection to the sample edges, the expulsion of lamellae in the intermediate state is continuous, while upon zero-field-cooling (ZFC) the flux penetration will be broken up by the geometrical energy barrier, which isolates the

flux tubes from the sample edges through a diamagnetic band [47]. The continuous expulsion of flux provides a possible way to control the vorticity of flux tubes.

To fit the fluxoid magnetic field, a monopole model is often used if the constraint $(r^2 + z_0^2) \gg \lambda_{ab}$ is satisfied [48–53], where r is the distance from the fluxoid center, z_0 is the height of the Hall probe to the sample surface and λ is the penetration depth. The magnetic field perpendicular to the sample surface $B_z(r, z_0)$ is expressed as:

$$B_z(r, z_0) = \frac{\Phi}{2\pi} \frac{z_0 + \lambda}{\left[r^2 + (z_0 + \lambda)^2\right]^{3/2}} \tag{5.3}$$

where Φ is the total flux bounded in a fluxoid. According to Ref. [54], the accuracy of the model can be enhanced by averaging over an area representative of the Hall probe active area to account for the convolution of the field over the probe. The integration of Equation (5.3) over a square active area of size s and divided by the area s^2 gives the following result:

$$B(x, y, z_0) = \frac{\Phi}{2\pi s^2} \int_{y-\frac{s}{2}}^{y+\frac{s}{2}} dy \int_{x-\frac{s}{2}}^{x+\frac{s}{2}} dx \frac{Z}{\left[x^2 + y^2 + Z^2\right]^{3/2}} \tag{5.4}$$

where $Z = z_0 + \lambda_{ab}$. For our SHPM, a Hall probe with an active area of $s^2 = 0.4 \times 0.4\ \mu m^2$ is used.

Figure 5.6a shows a typical SHPM image of the flux tube state observed after FC at $H = 7$ Oe and $T = 4.2$ K. Seven fluxoids with different sizes are observed in the scanned area. Cross sections (filled symbols) of fluxoid I and II along the solid white lines in

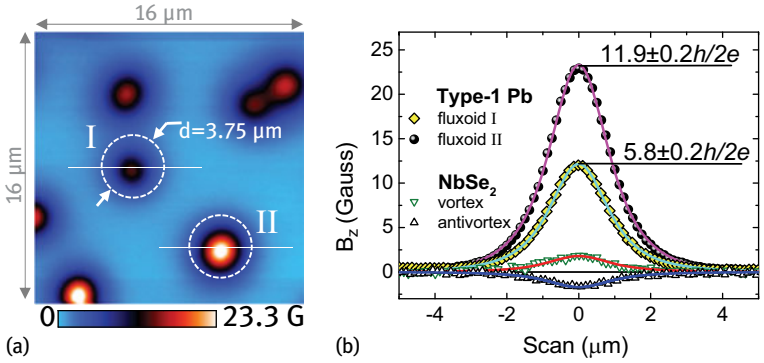

Fig. 5.6: (a) SHPM image obtained after FC at $H = 7$ Oe and $T = 4.2$ K for a type-I lead film. The dashed circles show the area chosen for integration. (b) 2D fit (solid lines) to the data (filled symbols) from cross sections of the flux tubes as shown by the white lines in the SHPM image of Figure 5.6a. The fits give (I) $Z = 1.237\ \mu m$ and $\Phi = 5.8 \pm 0.2\ h/2e$ and (II) $Z = 1.266\ \mu m$ and $\Phi = 11.9 \pm 0.2\ h/2e$. The open symbols show the cross sections of a vortex and an antivortex observed in a reference $NbSe_2$ single crystal.

Figure 5.6a are demonstrated in Figure 5.6b. The best fitting using Equation (5.4) gives (I) $Z = 1.237\,\mu m$, $\Phi = 5.8 \pm 0.2\, h/2e$ and (II) $Z = 1.266\,\mu m$, $\Phi = 11.9 \pm 0.2\, h/2e$, respectively. For comparison, in Figure 5.6b, the cross sections of a vortex and an antivortex observed in a reference $NbSe_2$ single crystal at $T = 4.2$ K is shown. The fitting gives an average $\Phi = 0.95 \pm 0.2\, h/2e$. By introducing an effective flux quantum [55] to compensate the loss of magnetic flux due to a stray magnetic field, the vorticity of flux tubes is also confirmed by integrating the magnetic signal of the flux tube in a limited area, for example, as indicated in Figure 5.6a by the dashed circle. The integration results in very consistent values with the monopole model fitting.

With the monopole model introduced above, we are able to quantify the fluxoids in the intermediate state. In the following, we consider the tubular state observed from two approaches: flux penetration and flux expulsion.

5.4.3.1 Flux penetration

In Figure 5.7 we show the observed flux tubes induced through the flux penetration process after ZFC to 6.9 K. Below $H = 2$ Oe, the sample remains in the Meissner state. At $H = 2.6$ Oe, the first flux tube is observed in the scanned area (Figure 5.7a). With increasing field, more and more flux tubes penetrate the scanned area (Figure 5.7a–d), and eventually they will merge and start forming stripes [56]. The minimum flux tube observed at $T = 6.9$ K, as shown by the dashed circles, contains four flux quanta ($L_{min} = 4$). Looking at the temperature dependence of L_{min}, we have observed that L_{min} increases with decreasing temperature as shown in Figure 5.7e. These observations are in agreement with the impeded flux penetration scenario. According to Refs.[47] and [37], the penetration of magnetic flux in the intermediate state of a type-I superconductor is impeded. This implies that the vortices will first accumulate at the sample border to form flux tubes, once the flux tubes contain a large enough amount of magnetic flux as to overcome the surface barrier, they will burst into the sample interior pushed by the Meissner currents. Therefore, our data give an indirect evidence for the impeded flux penetration. As observed, at lower temperatures, due to an increase of the surface energy barrier, the minimum flux tube is expected to contain multiple flux quanta to overcome the energy barrier. Figure 5.7e shows the penetration field H_p as a function of temperature. It is clear that with decreasing temperature, the penetration field increases due to the enhanced surface energy barrier. Therefore, the minimum fluxoid also increases. We notice that the flux tubes may contain a slightly different number of flux quanta; this is probably due to the presence of small edge imperfections which yield slightly different energy barriers.

Experimentally, no single quantum vortex has been observed through flux penetration, but it cannot be ruled out at high temperatures, especially close to the normal-intermediate transition. This is a process that still needs further investigation.

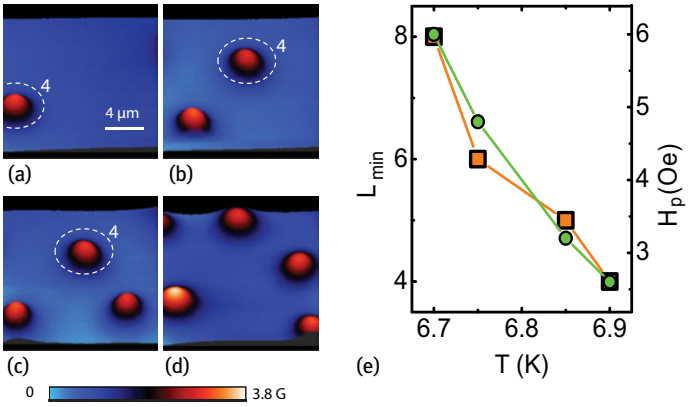

Fig. 5.7: SHPM images taken after first performing ZFC to 6.9 K and subsequently increasing the magnetic field to: (a) 2.6 Oe; (b) 2.8 Oe; (c) 3 Oe; (d) 3.4 Oe. The minimum flux tube observed contains four flux quanta as shown by the dashed circles with the vorticity indicated beside it. (e) Penetration field H_p (circles) and the vorticity of minimum fluxoid (squares) as a function of temperature.

5.4.3.2 Flux expulsion

Figure 5.8 shows the SHPM images measured at 6.5 K after FC under various magnetic fields. Above $H = 0.2$ Oe, the fluxoid, indicated by the dashed circle, nucleates in the scanned area. The vorticity of the fluxoid, shown by the number near the circle, is determined from both fitting and integration. Figure 5.8k shows the result of integration for the flux tube observed at different cooling fields. Below $H = 0.2$ Oe, no fluxoid is formed. A single flux quantum is observed in the field range of $0.2\ Oe \leqslant H < 0.4$ Oe. With increasing cooling field, the vorticity increases up to $L = 7$ at $H = 0.95$ Oe. In Figure 5.8l we show cross sections of seven singly quantized fluxoids. The fit by the monopole model yields $\Phi = 0.96\, h/2e$ as shown by the solid line.

The observation of a single flux quantum in such a macroscopic sample is quite surprising. In the intermediate state of type-I superconductors, the energy of singly quantized vortices is larger than the energy of multiply quantized flux tubes, which favors an unstable state if it is composed of Φ_0 fluxoids. It should be noted that the single flux quantum observed here has to be stabilized by a different mechanism from those considered in Ref. [45] and [46], where the formation of individual vortices is due to the strong geometrical confinement, and individual vortices are observed in both flux penetration and expulsion processes for the type-I nanowires [46]. In macroscopic type-I superconductors, the intermediate state is a result of the competition between the magnetic energy that favors the formation of small normal domains and the positive surface energy that tends to form large domains. It has been argued that in mesoscopic type-I samples a third interaction, provided by the confinement effect of the sample boundaries, is responsible for the stabilization of single-quantum fluxoids [45]. However, in our film (with lateral dimension 1×1 cm and $d = 5$ μm), the

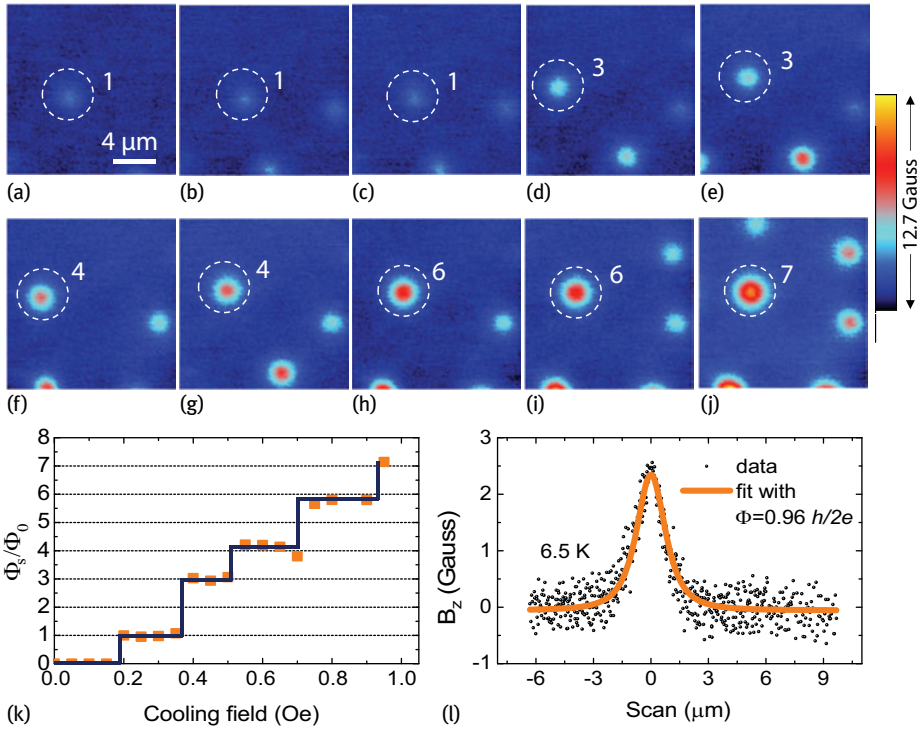

Fig. 5.8: SHPM images observed after FC to 6.5 K at various magnetic fields: (a) 0.25 Oe; (b) 0.3 Oe; (c) 0.35 Oe; (d) 0.4 Oe; (e) 0.5 Oe; (f) 0.6 Oe; (g) 0.65; (h) 0.75 Oe; (i) 0.9 Oe; (j) 1.2 Oe. The dashed white circles show the positions of the fluxoids with the numbers on top indicating their vorticity. (k) Normalized smallest vortex flux Φ_s as a function of applied field. The solid line is a guide to the eyes. (l) Cross sections of five fluxoids observed below 0.4 Oe. The best fit(solid line) gives $\Phi = 0.96\, h/2e$.

geometrical confinement effect on the flux tubes has to be very weak. We argue that the stabilization of singly quantized fluxoids in a macroscopic type-I superconductor is possible due to the extra interaction introduced in the system by a weak collective pinning landscape, playing a similar role as the extra interaction introduced in mesoscopic samples due to geometry confinement [57, 58].

5.4.4 Dynamics of flux patterns

To study the stability and dynamics of vortex states, many different setups have been used, such as magnetic force microscopy [59], scanning superconducting quantum interference device (SQUID) microscopy [60] and scanning ac-susceptibility microscopy [61–63]. Compared with other techniques, the ac-susceptibility technique has the advantage of measuring the vortex dynamics at a higher flux density in a

relatively large area. By applying an ac field with various amplitudes, the SSM allows one to shake the flux lines periodically by the Lorentz force raised by the induced currents, while at the same time one can directly image the equilibrium flux patterns and record locally the in-phase and out-of-phase magnetic response.

From the phase diagram in Figure 5.5a, we see that the flux tube state observed after flux penetration is divided into two parts by the phase boundary H_s' of flux expulsion. Different vortex dynamics are expected for the two regions. In the following discussion, the tubular state between H_p and $H_s^{'}$ is defined as the low-density flux tube phase (LDFTP), while the region between $H_s^{'}$ and H_s is called the high-density flux tube phase (HDFTP).

5.4.4.1 Low-density flux tube phase

Figure 5.9a shows the SHPM images of a LDFTP taken at $H = 6$ Oe after performing a ZFC down to 6.9 K. The initial flux pattern (Figure 5.9a) is metastable, and the position of flux tubes keep on evolving over time (up to 2 hours). When applying an ac field with the amplitude $h_{ac} = 0.5$ Oe and frequency $f = 25.123$ Hz, the pattern changes (Figure 5.9b) to incorporate a new flux distribution where tubes oscillate around their newly defined equilibrium positions (marked as dots in Figure 5.9b). The right panel of Figure 5.9b shows the in-phase SSM image, it is clearly seen that around each equilibrium position a red (to the left of the equilibrium position) and a blue (to the right of the equilibrium position) spot is observed. Where a red spot appears it means that a flux tube has moved into that spot upon increasing h_{ac}, while where a blue spot appears it means that a flux tube has moved out of that position upon increasing h_{ac}. It is expected that the more the flux tube is displaced from its equilibrium position the more intense is the in-phase signal.

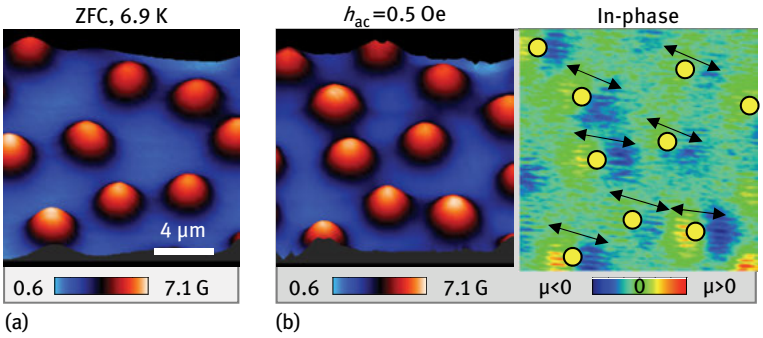

Fig. 5.9: (a) SHPM image measured at $H = 6$ Oe after ZFC to 6.9 K. (b) Dc and in-phase images taken at $H = 6$ Oe and $h_{ac} = 0.5$ Oe. Dots indicate the average position of flux tubes in the dc image. The arrows show the oscillation direction for the flux tubes.

The resulting oscillatory movement (depicted by the arrows) bears a close resemblance to the Campbell oscillatory behavior of a vortex lattice in the mixed state of a type-II/2 superconductor [62]. After switching the ac field off, the vortex pattern freezes in the new equilibrium position, shown by Figure 5.9b, which, in turn, does not demonstrate any variation over time or even when applying further shaking with $h_{ac} = 0.5$ Oe. Only when a higher h_{ac} or H_{dc} is applied, do the flux tubes have enough energy to overcome their pinning potentials. A similar response was first observed by Goren and Tinkham when applying a driving current through a stripe of a type-I superconducting indium film [36]. Notice that by superimposing an ac field to the LDFTP the flux tubes gain enough mobility to quickly reach an equilibrium position which otherwise takes a long time to approach. The increase in mobility observed due to the superposition of an ac field has been previously reported for a type-I superconductor [64] and has a strong similarity to the mixed state of a type-II/2 superconductor under the action of an ac field [65].

Typically in type-II/2 superconductors each vortex carries only one flux quantum [66] and they experience a repulsive vortex-vortex interaction, while the flux tubes in a type-I superconductor are composed of a multiple integer number of flux quanta and they demonstrate a short-range attractive interaction and a long-range weak repulsive interaction. Hence, it is natural to expect different dynamics in these systems. However, in the LDFTP a similar dynamical behavior between flux tubes and vortices in the mixed state of type-II/2 superconductors is obtained, where the vortices oscillate around their pinning potentials under a low ac field and jump from one to another at high enough ac fields [62]. Also notice that the flux tubes in the LDFTP have similar diameters, and the fitting with the monopole model gives a vorticity of $L \approx 7\Phi_0$ for each flux tube. This indicates that all flux tubes contain a similar number of flux quanta, suggesting that the initial change of the observed tubular pattern (Figure 5.9b) is not due to the split of the original flux tubes but rather due to the rearrangement of the flux lattice. Moreover, as will be further discussed, the increase in stability of the resulting tubular patterns that occurs after applying the ac field is the result of a dynamical process that allows the flux tubes to be trapped by the randomly located pinning centers.

5.4.4.2 High-density flux tube phase

Figure 5.10a shows a pattern of flux tubes in the dashed area of the phase diagram in Figure 5.5a. If applying a small h_{ac}, the in-phase SSM image (Figure 5.10b lower panel) shows that the flux tubes oscillate around their equilibrium positions. It should be noted that here the flux tubes are inhomogeneous in size (and magnetic field intensity) and some of them are not round but present in an elliptical shape, still their dynamical behavior under a gentle ac-shake is similar to that obtained in the LDFTP. Nevertheless, in the HDFTP the h_{ac} needed to set the flux into motion is lower than that in the LDFTP due to the stronger interaction among the flux tubes which adapts

the whole flux pattern better to available pinning centers. It is therefore suggested that the increase in the interaction between flux tubes is the origin of the stability observed in the HDFTP during the flux penetration experiments. A similar effect is also reported in the peak effect regime of type-II superconductors, which is ascribed to the collective pinning due to the softening of the elastic moduli of the vortex lattice [67].

By increasing the ac field, the vortex pattern starts to change, part of the flux tubes combine and then they stabilize again (Figure 5.10c), indicating that the "dither force" is still not strong enough to totally overcome collective interactions. When further increasing the "dither force" up to a critical value (h_{ac} = 0.3 Oe for this dc field and temperature), the dragging force applied to the flux tubes overcomes the equilibrium interaction among them and the flux tubes move by splitting and recombining as shown in Figure 5.10d. No stable vortex pattern can be observed. After switching the ac field off the vortex pattern has reconfigured into a coexistence state of stripes and flux tubes (Figure 5.10e). To verify that the observed flux pattern reconfiguration results from a dynamical effect and not because of increasing the flux by applying the ac field ($H_{dc} + h_{ac}$), the SHPM images were measured at 6.9 K after ZFC and then progressively increasing the external field H_{dc} from 10 Oe to 10.5 Oe. Only minor changes in the vortex patterns are seen even at 10.5 Oe, thus supporting the suggestion that the reorganization of flux observed by applying an ac field in the HDFTP reflects an intrinsic dynamical behavior.

When further shaking the stripe pattern with a higher ac field, the stripes may rearrange into another form. However, they never break into flux tubes [68]. This looks quite natural because the tubular flux pattern is constrained by the collective pinning

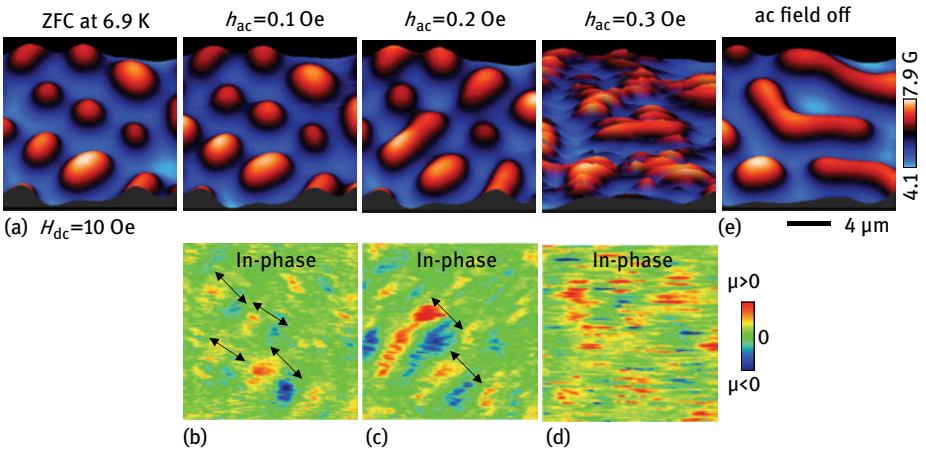

Fig. 5.10: (a) High-density flux tube state obtained at H_{dc} = 10 Oe after ZFC to 6.9 K. SHPM (upper panel) and SSM (lower panel) images obtained at various oscillating fields: (b) h_{ac} = 0.1 Oe, (c) h_{ac} = 0.2 Oe and (d) h_{ac} = 0.3 Oe. The arrows show the oscillating direction of the flux tubes. (e) SHPM image taken after switching off the ac field.

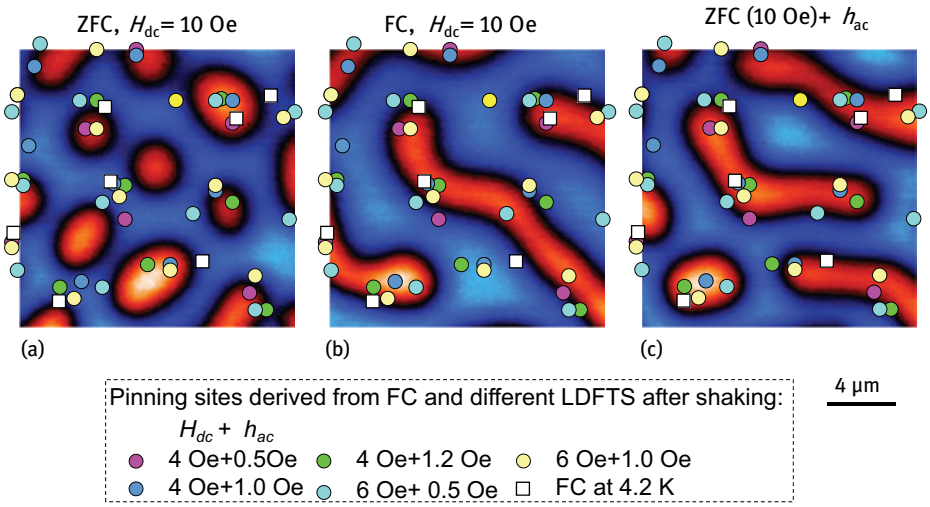

Fig. 5.11: Vortex patterns obtained at 6.9 K with H_{dc} = 10 Oe after performing: (a) ZFC; (b) FC; (c) after shaking the vortex pattern of ZFC. The dots indicate the randomly distributed pinning centers derived from the equilibrium patterns of a low-density flux tube state. The squares show the positions of flux tubes derived from FC at 4.2 K.

to a lot of metastable states which may have a higher free energy than the equilibrium state. Since the free energy difference between the tubular state and the stripe state is quite small [69], after increasing the static field the tubular pattern has enough time to adapt to another metastable tubular state in order to compensate the energy increase due to the increased field (a superheated tubular state). However, when applying an ac field, the tubular pattern cannot follow the rate of change of the magnetic field, i.e., before it reaches another metastable tubular pattern, the field changes again. Then all the patterns are gradually pushed into a state with a much higher energy which is unstable. After switching the ac field off, all the flux domains reorganize down to the most energetically favorable state, which for this field and temperature is the stripe pattern as previously shown by the flux expulsion experiments.

5.4.4.3 Stability of various flux states

The dynamical rearrangement of the flux domains and the FC experiments suggests that above a certain field, which is temperature dependent, the stripe pattern favors a lower energy state compared to the flux tubes. This is totally in contrast to the case in a pinning-free sample, where the tubular pattern represents the topological equilibrium state [69] for all magnetic fields. To unveil the mechanism behind the rearrangement of flux domains, Figure 5.11 presents the vortex patterns obtained at the same parameters (6.9 K, 10 Oe) after different approaches: (a) ZFC; (b) FC; (c) ZFC + h_{ac}. The intrinsic pinning potentials are also shown by the dots and the squares. The dots are derived

from the equilibrium patterns of the LDFTP after shaking with various ac fields (e.g., Figure 5.9c), while the squares indicate the positions of pinned flux tubes after FCs at $T = 4.2$ K. The overlap of the pinning centers, obtained from different runs further proves the claim that after gently shaking with an h_{ac} all the flux tubes stabilize at the pinning centers.

From Figure 5.11a, it is seen that the flux tubes are randomly distributed after a ZFC, with only a few of them sitting at the pinning centers (40%) which favors the picture of a superheated flux tube state stabilized by their collective interaction. However, when expelling flux out of the sample by performing field-cooling, the stripe-like normal domains nucleate with 87% of pinning potentials occupied by the normal domains (Figure 5.11b). This ensures a more stable state compared to that of flux penetration (Figure 5.11a). Also in Figure 5.11c, the reconfigured flux tube state forms after shaking pattern Figure 5.11a with an $h_{ac} = 0.3$ Oe as formerly discussed. It is found that 92% of the pinning sites are well occupied by the normal domains, which shows the effect similar to the FC process. Note that performing the same experiments at different locations gives consistent results although the pinning distribution varies from scanning areas. This is reminiscent of the recent report on the inverse melting of the vortex lattice in high T_c superconductors [70], where by applying a big enough ac field, magnetic hysteresis disappears. Therefore, a reduction or even the disappearance of hysteresis is also expected in a macroscopic M-H loop with the ac field on.

5.5 Type-II/1 superconductor with short-range repulsive and long-range attractive v-v interaction

Although discovered more than half a century ago, type-II/1 superconductors are the least known ones among all kinds of superconductors. Early research based on Bitter decoration has revealed that the vortex pattern is composed of large areas of Meissner state and vortex clusters. However, detailed studies of the transition from type-II/1 to type-II/2 or type-I, with single-vortex resolution, have rarely been performed. This might be due to the lack of type-II/1 superconductors and the proper technique to probe them. In this section, we introduce the study of vortex pattern evolution in a type-II/1 superconductor simply by changing the temperature.

5.5.1 Vortex phase diagram

The sample used in the study is a ZrB_{12} single crystal with a κ in the range of 0.8–1.12 [71, 72]. Hence, from the κ–T phase diagram, a phase transition from type-II/1 to type-II/2 is expected by varying the temperature. Figure 5.12e presents the virgin $M(H)$ curves at various temperatures. It is clear that below H_{c1} the sample is in the Meissner state. At H_{c1} the $M(H)$ curves exhibit an abrupt jump ΔM and the magnetic field

penetrates the sample to form the intermediate mixed state. When the magnetic field reaches H^*, another discontinuity appears, then M gradually decreases to 0 at H_{c2}. With increasing temperature, the magnetization jump ΔM is suppressed and the traditional type-II/2 behavior dominates [73]. This can better be seen from Figure 5.12b where ΔM follows a linear dependence with temperature as indicated by the solid line, and above $T^* = 0.97 \pm 0.01 T_c$, ΔM decreases to zero, indicating that the repulsive interaction prevails. The observed behavior is very similar to another type-II/1 superconductor Nb [74]. The phase diagram deduced from the above is shown in Figure 5.12c. Three magnetic phases are observed, with the IMS only occupying a narrow area in the phase diagram. However, it should be noted that, due to the existence of a surface barrier and random pinning produced by the quenched disorder, the vortex patterns nucleated above H_{c1} can still be observed even when entering the Meissner state by, for example, performing a field-cooling (FC) process.

5.5.2 Vortex pattern evolution

The evolution of the vortex patterns for an FC regime under a magnetic field of 4.73 Oe is shown in Figure 5.13. The bright red spots represent vortices, while the intervortex superconducting state is displayed as dark areas. At 5.82 K the Abrikosov vortex lattice is well formed indicating the sample is in the traditional type-II/2 regime. Note that the triangular vortex lattice is distorted, due to the existence of quenched disor-

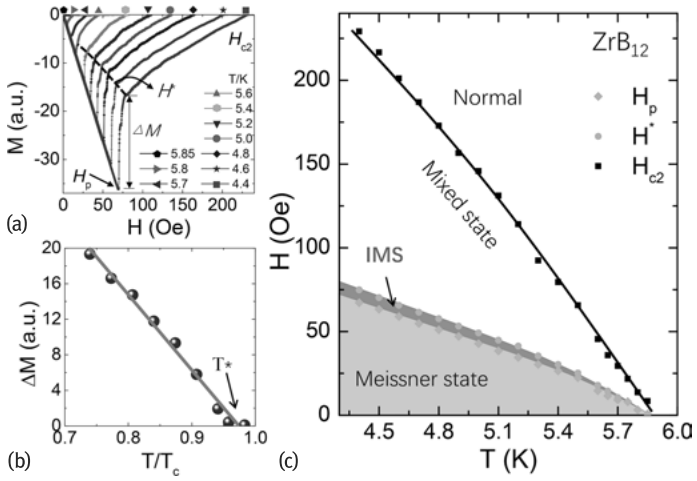

Fig. 5.12: (a) Magnetization curve for ZrB_{12} at various temperatures. The dashed line marks the position of H_c, above which type-II behavior dominates. (b) The magnetization jump at H_{c1} as a function of reduced temperature. By extrapolating the linear dependence, ΔM disappears at $T^* = 0.97 \pm 0.01 T_c$. (c) H–T phase diagram showing different regimes of vortex phases, where the type-II/1 (IMS) regime only occupies a narrow area.

der. In some other areas with less defects, a well-ordered triangular lattice is formed at high temperatures. With decreasing temperature, the vortex lattice becomes more and more disordered as a result of the increase of the attractive interactions among vortices. At intermediate temperatures, a square lattice is energetically favorable as shown by the white circles at 5.67 K and 5.6 K. This is also supported by the vortex pattern evolution as a function of time. The results are presented in Figure 5.14. After first cooling down to 5.7 K, part of the vortices still remain in the triangular lattice, as highlighted by the symbols. After waiting for 5 minutes, the triangular vortex lattice rearranges to a square lattice and stabilizes (as displayed in Figure 5.14b, which is measured 5 minutes after Figure 5.14a). This provides direct evidence that the square lattice is energetically more stable than the triangular lattice when the vortex attraction appears. A square lattice has also been suggested for another low-κ material (Nb) from neutron diffraction measurements [75]. At even lower temperatures, vortices finally form vortex chains and clusters, as indicated by the open symbols and dashed oval, respectively, in Figure 5.13a. This order-disorder transition can be reversed by warming up the sample across the phase boundaries as presented in Figure 5.13b.

The formation of vortex chains is quite interesting. A similar phenomenon has been observed in many physical systems with competing interactions. For example, in the transition from the vortex solid to the vortex liquid phase, the thermal fluctu-

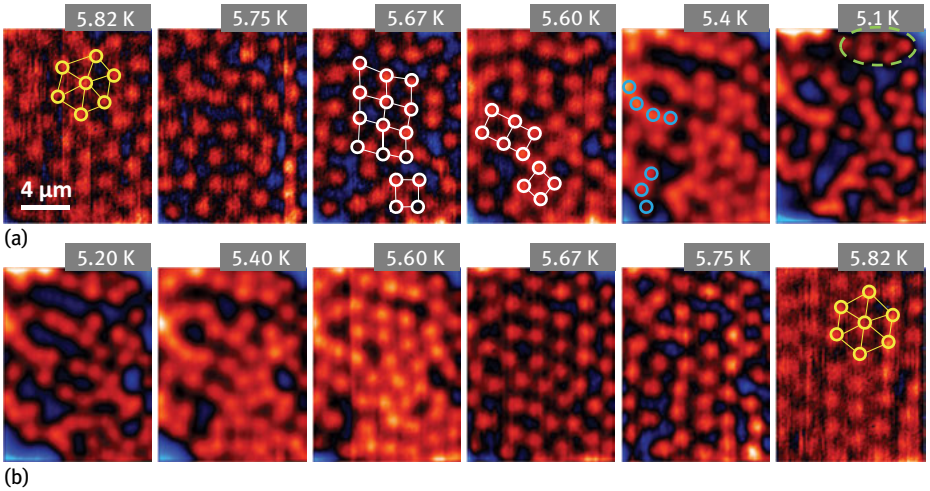

Fig. 5.13: Vortex pattern evolution with cycling temperature after FC at $H = 4.73$ Oe. (a) SHPM images observed with decreasing temperature. The bright red spots represent vortices. A distorted triangular vortex lattice is observed at 5.82 K as highlighted by the symbols. With decreasing temperature, vortices tend to form a square lattice, as indicated by the white squares, and then transform to a disordered state with vortex chains (open symbols) and clusters (dashed oval) as can be seen at 5.4 K and 5.1 K. (b) When cycling the temperature back, a disorder-to-order transition of the vortex arrangement is recovered.

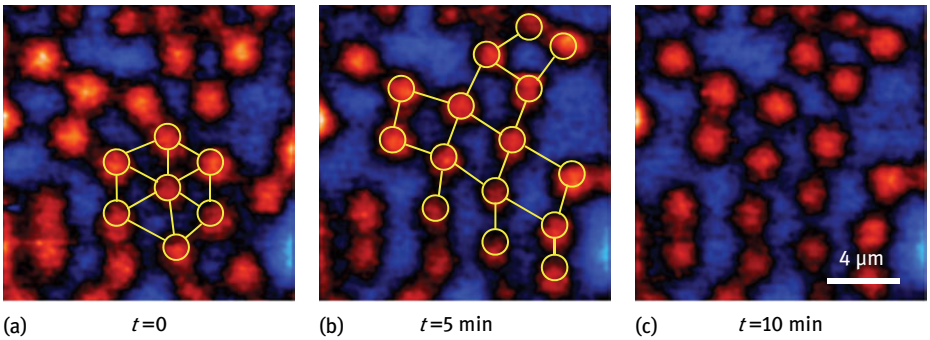

Fig. 5.14: Formation of square lattice. (a) SHPM image measured after FC to 5.7 K at $H = 1.5$ Oe. Part of the vortices still remain in the triangular lattice as indicated by the open symbols. SHPM images taken (b) five minutes and (c) ten minutes after (a). The vortices rearrange into a square lattice.

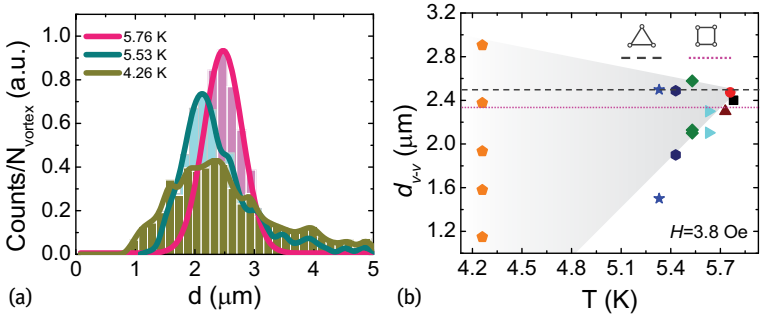

Fig. 5.15: (a) Statistics of the nearest-neighbor distances for the vortex patterns at various temperatures. (b) Nearest-neighbor distance at the peak position as a function of temperature. The shaded area indicates the peak distribution width, which increases with decreasing temperature. The dashed and dotted lines correspond to the nearest-neighbor distance for a triangular and square lattice, respectively.

ations overcome the vortex repulsive interaction and a linear vortex arrangement appears [76]. Here, the competition arises from the short-range repulsive and long-range attractive interactions. A close resemblance has also been found compared to the vortex patterns in the type-1.5 superconductor MgB_2, where vortex stripes and clusters are formed under the competition of long-range attraction and short-range repulsion between vortices due to the two-band effect [3, 4, 18, 77].

The distribution of the first-neighbor distances $d_{v\text{-}v}$ for a large vortex pattern is calculated for both the ordered and disordered state and is plotted in Figure 5.15a. The vortex distribution for the ordered state can be fitted by a Gaussian form with the maximum around 2.47 muupm, which is consistent with the value ($\sim$ 2.5 muupm) from the triangular vortex lattice at the same field by using $d^2_{v\text{-}v} = 2\phi_0/\sqrt{3}B$. In contrast, the disordered state shows a much broader distribution with additional peaks being

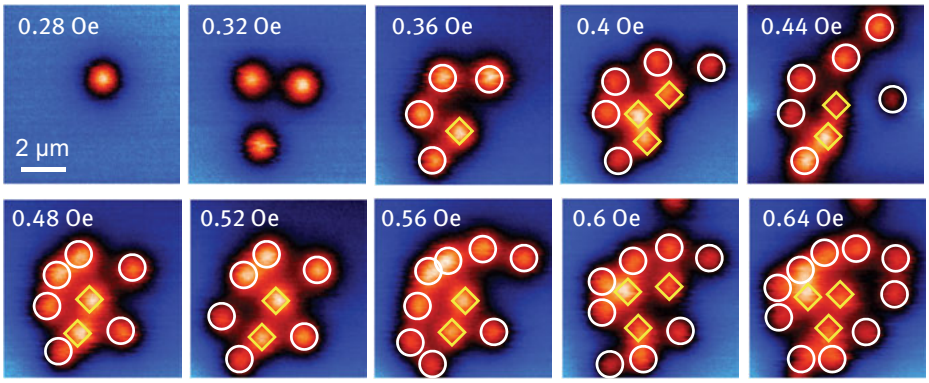

Fig. 5.16: SHPM images observed after FC with progressively increasing magnetic fields, showing the formation of a vortex cluster. The diamonds indicate the location of the pinned core vortices, while the circles indicate the positions of fringe vortices attracted to the pinned ones.

observed. The distances corresponding to the observed vortex distribution peaks are displayed in Figure 5.15b. It is seen that, with decreasing temperature, the minimum $d_{v\text{-}v}$ value at the peaks decreases while the peak distribution width (shown by the shaded area) increases. These results provide direct evidence for the attractive interactions between vortices at low temperatures.

5.5.3 Vortex clusters in the IMS

Another important feature of the IMS is the formation of vortex clusters, which have been observed all over the IMS in ZrB_{12}. However, there is no ordering of the clusters. Figure 5.16 presents the formation process of a typical vortex cluster. The vortices are shown by using different symbols: 1) Core vortices by the diamonds. These are the vortices located close to the pinning centers. After each field-cooling, they always prefer to nucleate around the same locations. These vortices form the cluster cores. 2) Fringe vortices marked by the open circles. These vortices nucleate around the core vortices at high temperatures and subsequently are pushed to them by the appearance of attractive interaction when cooling down to the type-II/1 regime. Fringe vortices (circles) tend to form the triangular arrangement with core vortices (diamonds), forming the periphery of the clusters. In this scenario, the vortex clusters can still be regarded as a distorted Abrikosov vortex lattice. Notice, however, that the first-neighbor distance inside the cluster remains constant as the field is increased, with a value of 1.9 muupm. In the IMS of clean low-κ superconductors, Meissner areas appear surrounded by mixed-state areas presenting a triangular vortex lattice with constant vortex-vortex separation. The same trend is found within the vortex clusters although they are highly disordered due to the presence of weak pinning in the sam-

ple. Additionally, it should be noted that no giant vortices are formed in the vortex cluster, suggesting that the repulsive force dominates at short distances and in this temperature range.

5.6 Conclusions and outlook

To summarize, the feasibility of introducing and manipulating the interactions make superconductors (type-I and type-II/1) a perfect platform to study modulated systems. The study of vortex matter in different superconducting systems will definitely promote new research of similar modulated systems. This opens new possibilities not only within the superconducting community but also for researchers working in other areas like astrophysics, ferrofluids, liquid crystals and so on. Lastly, we would like to give an outlook on future work:

1. So far, the study of type-I superconductors is mainly performed on plain films and singe crystals, where pinning centers are randomly distributed in the materials during the sample preparation. Further work on samples with artificial periodic pinning arrays would definitely add new richness to the system. For instance, in a type-I superconductor with periodic pinning centers, one might be able to stabilize $\Phi_0, 2\Phi_0, 3\Phi_0 \ldots$ vortex lattices under certain parameters. The matching effect observed in type-II superconductors might also be dramatically changed.
2. It would be interesting to study a superconductor with κ slightly smaller than $1/\sqrt{2}$. Since in this region, a transition from the type-II/1 to type-I phase will occur with varying temperature and the related vortex interactions become totally opposite (from long-range attractive and short-range repulsive to long-range repulsive and short-range attractive). Such a measurement has never been done so far, and a lot remains unclear. To facilitate this, films of type-I superconductor with various thickness could be perfect candidates. In superconducting films with the thickness d comparable or smaller than the bulk penetration depth (λ), the effective Ginzburg–Landau parameter κ_{eff} will mainly be determined by the effective penetration depth $\kappa_{\text{eff}} = \Lambda/\xi = \lambda^2/d\xi$. Therefore, κ_{eff} can be easily manipulated by changing thickness of the film. Such study will eventually bridge type-I and traditional type-II superconductors.
3. The recently discovered type-1.5 superconductivity in two and multigap superconductors provides a new way to study vortex competitions, especially in superconductor heterostructures.

Acknowledgment: We acknowledge the support from FWO and the Methusalem funding by the Flemish government. This work is also supported by the MP1201 COST action.

Bibliography

[1] Seul M, Andelman D. Domain shapes and patterns: The phenomenology of modulated phases. Science, 267(5197):476–483, 1995.

[2] Jacobs AE. First-Order Transitions at H_{c1} and H_{c2} in Type-II Superconductors. Phys. Rev. B, 4(9):3022, 1971.

[3] Babaev E, Speight M. Semi-Meissner state and neither type-I nor type-II superconductivity in multicomponent superconductors. Phys. Rev. B, 72(18):180502, 2005.

[4] Moshchalkov VV, Menghini M, Nishio T, Chen QH, Silhanek AV, Dao VH, Chibotaru LF, Zhigadlo ND, Karpinski J. Type-1.5 Superconductivity. Phys. Rev. Lett. 102:117001, 2009.

[5] Ray D, Olson Reichhardt CJ, Janko B, Reichhardt C. Strongly Enhanced Pinning of Magnetic Vortices in Type-II Superconductors by Conformal Crystal Arrays. Phys. Rev. Lett. 110:267001, 2013.

[6] Chibotaru LF, Ceulemans A, Bruyndoncx V, Moshchalkov VV. Symmetry-induced formation of antivortices in mesoscopic superconductors. Nature, 408(6814):833–835, 2000.

[7] Komendova L, Milosevic MV, Peeters FM. Soft vortex matter in a type-I/type-II superconducting bilayer. Phys. Rev. B, 88(9):094515, 2013.

[8] Alloul H, Lyle S. Introduction to the Physics of Electrons in Solids. Springer Science & Business Media, Heidelberg, 2010.

[9] Krageloh U. Flux line lattices in the intermediate state of superconductors with Ginzburg Landau parameters near $1/\sqrt{2}$. Phys. Lett. A, 28(9):657–658, 1969.

[10] Essmann U. Observation of the mixed state. Physica 55:83–93, 1971.

[11] Aston DR, Dubeck LW, Rothwarf F. Intermediate Mixed State of Type-II Superconductors. Phys. Rev. B, 3(7):2231, 1971.

[12] Auer J, Ullmaier H. Magnetic Behavior of Type-II Superconductors with Small Ginzburg–Landau Parameters. Phys. Rev. B 7:136–145, 1973.

[13] Eilenberger G, Buttner H. The structure of single vortices in type-II superconductors. Z. Phys., 224(4):335–352, 1969.

[14] Dichtel K. A nonlocal model of a single flux line. Phys. Lett. A, 35(4):285–286, 1971.

[15] Halbritter J. On the penetration of the magnetic field into a superconductor. Z. Phys., 243(3):201–219, 1971.

[16] Leung MC, Jacobs AE. Asymptotic behavior of the vector potential and the order parameter for an isolated vortex. J. Low Temp. Phys., 11(3–4):395–419, 1973.

[17] Leung MC. Attractive interaction between vortices in type-II superconductors at arbitrary temperatures. J. Low Temp. Phys., 12(1–2):215–235, 1973.

[18] Gutierrez J, Raes B, Silhanek AV, Li LJ, Zhigadlo ND, Karpinski J, Tempere J, Moshchalkov VV. Scanning Hall probe microscopy of unconventional vortex patterns in the two-gap MgB_2 superconductor. Phys. Rev. B 85:094511, 2012.

[19] Nishio T, Dao VH, Chen Q, Chibotaru LF, Kadowaki K, Moshchalkov VV. Scanning squid microscopy of vortex clusters in multiband superconductors. Phys. Rev. B 81:020506, 2010.

[20] Babaev E, Garaud J, Agterberg D. Vortex coalescence and type-1.5 superconductivity in Sr_2RuO_4. APS Meeting Abstracts 1:35014, 2013.

[21] Ray SJ, Gibbs AS, Bending SJ, Curran PJ, Egor Babaev, Baines C, Mackenzie AP, Lee SL. Muon-spin rotation measurements of the vortex state in sr_2ruo_4: Type-1.5 superconductivity, vortex clustering, and a crossover from a triangular to a square vortex lattice. Phys. Rev. B, 89(9):094504, 2014.

[22] Komendová L, Milošević MV, Peeters FM. Soft vortex matter in a type-i/type-ii superconducting bilayer. Phys. Rev. B 88:094515, 2013.

[23] Varney CN, Sellin KAH, Wang Q-Z, Fangohr H, Babaev E. Journal of Physics: Condensed Matter 25(41): 415702, 2013.
[24] Ge J, Gutierrez J, Li J, Yuan J, Wang H-B, Yamaura K, Takayama-Muromachi E, Moshchalkov VV. Peak effect in optimally doped p-type single-crystal $Ba_{0.5}K_{0.5}Fe_2As_2$ studied by ac magnetization measurements. Phys. Rev. B, 88(14):144505, 2013.
[25] Ge J, Gutierrez J, Li J, Yuan J, Wang H-B, Yamaura K, Takayama-Muromachi E, Moshchalkov VV. Dependence of the flux-creep activation energy on current density and magnetic field for a $Ca_{10}(Pt_3As_8)[(Fe_{1-x}Pt_x)_2As_2]_5$ single crystal. Appl. Phys. Lett., 104(11):112603, 2014.
[26] Ge J, Gutierrez J, Li M, Zhang J, Moshchalkov VV. Vortex phase transition and isotropic flux dynamics in $K_{0.8}Fe_2Se_2$ single crystal lightly doped with Mn. Appl. Phys. Lett., 103(5):052602, 2013.
[27] Ge J, Gutierrez J, Raes B, Watanabe T, Koshio J, Moshchalkov VV. Two energy gaps in superconducting $Lu_2Fe_3Si_5$ single crystal derived from the temperature dependence of lower critical field $H_{c1}(T)$. Physica C 478:5–9, 2012.
[28] Zehetmayer M, Eisterer M, Jun J, Kazakov SM, Karpinski J, Wisniewski A, Weber HW. Mixed-state properties of superconducting mgb 2 single crystals. Physical Review B, 66(5):052505, 2002.
[29] Babaev E, Carlström J, Speight M. Type-1.5 superconducting state from an intrinsic proximity effect in two-band superconductors. Phys. Rev. Lett. 105:067003, Aug 2010.
[30] Malescio G, Pellicane P. Stripe phases from isotropic repulsive interactions. Nature Mat., 2(2):97–100, 2003.
[31] Diaz-Mendez R, Mezzacapo F, Lechner W, Cinti F, Babaev E, Pupillo G. Physical Review Letters 118:067001, 2017.
[32] Curran P, Desoky WM, Laloe JB, Bending SJ. Broken symmetry vortex structures in disordered MgB_2 thin films. Presentation at ICSM-2014 Conference, 2014.
[33] Bending SJ. Local magnetic probes of superconductors. Adv. Phys., 48(4):449–535, 1999.
[34] Hall EH. On a new action of the magnet on electric currents. Amer. J. Math., 2(3):287–292, 1879.
[35] Prozorov R. Equilibrium Topology of the Intermediate State in Type-I Superconductors of Different Shapes. Phys. Rev. Lett. 98:257001, 2007.
[36] Goren RN, Tinkham M. Patterns of magnetic flux penetration in superconducting films. J. Low Temp. Phys., 5(4):465–494, 1971.
[37] Berdiyorov GR, Hernandez-Nieves AD, Milosevic MV, Peeters FM, Dominguez D. Flux quantum discretized dynamics of magnetic flux entry, exit, and annihilation in current-driven mesoscopic type-I superconductors. Phys. Rev. B 85:092502, 2012.
[38] Tinkham M. Effect of Fluxoid Quantization on Transitions of Superconducting Films. Phys. Rev. 129:2413–2422, 1963.
[39] Maki K, Tsuzuki T. Magnetic Properties of Intrinsic London Superconductors. Phys. Rev., 139(3A):A868, 1965.
[40] Lasher G. Mixed State of Type-I Superconducting Films in a Perpendicular Magnetic Field. Phys. Rev. 154:345–348, 1967.
[41] Boersch H, Kunze U, Lischke B, Rodewald W. Observation of the mixed state in films of type-I superconductors (Pb). Phys. Lett. A, 44(4):273–274, 1973.
[42] Dolan GJ, Silcox J. Critical Thicknesses in Superconducting Thin Films. Phys. Rev. Lett. 30:603–606, 1973.
[43] Onori S, Rogani A. Thickness dependence of perpendicular critical fields in superconducting films of In, Pb and Sn. Physica B+ C, 132(2):217–222, 1985.
[44] Singh O, Curzon AE. Observation of the mixed state in single crystal lead films. Cryogenics, 15(11):665–666, 1975.

[45] Berdiyorov GR, Hernandez AD, Peeters FM. Confinement Effects on Intermediate-State Flux Patterns in Mesoscopic Type-I Superconductors. Phys. Rev. Lett. 103:267002, 2009.
[46] Engbarth MA, Bending SJ, Milosevic MV. Geometry-driven vortex states in type-I superconducting Pb nanowires. Phys. Rev. B 83:224504, 2011.
[47] Jeudy V, Gourdon C, Okada T. Impeded Growth of Magnetic Flux Bubbles in the Intermediate State Pattern of Type-I Superconductors. Phys. Rev. Lett. 92:147001, 2004.
[48] Nishio T, Chen Q, Gillijns W, De Keyser K, Vervaeke K, Moshchalkov VV. Scanning Hall probe microscopy of vortex patterns in a superconducting microsquare. Phys. Rev. B 77:012502, 2008.
[49] Wynn JC, Bonn DA, Gardner BW, Lin Y-J, Liang R, Hardy WN, Kirtley JR, Moler KA. Limits on Spin-Charge Separation from h/2 e Fluxoids in Very Underdoped $YBa_2Cu_3O_{6+x}$. Phys. Rev. Lett., 87(19):197002, 2001.
[50] Chang AM, Hallen HD, Harriott L, Hess HF, Kao HL, Kwo J, Miller RE, Wolfe R, Van der Ziel J, Chang TY. Scanning Hall probe microscopy. Appl. Phys. Lett., 61(16):1974–1976, 1992.
[51] Ge J-Y, Gutierrez J, Gladilin VN, Devreese JT, Moshchalkov VV. Bound vortex dipoles generated at pinning centres by Meissner current. Nature communications, 6, 2015.
[52] Gladilin VN, Ge J, Gutierrez J, Timmermans M, Van de Vondel J, Tempere J, Devreese JT, Moshchalkov VV. Vortices in a wedge made of a type-I superconductor. New J. Phys., 17(6):063032, 2015.
[53] Ge J, Gladilin VN, Xue C, Tempere J, Devreese JT, Van de Vondel J, Zhou Y, Moshchalkov VV. Magnetic dipoles at topological defects in the Meissner state of a nanostructured superconductor. Phys. Rev. B, 93(22):224502, 2016.
[54] Guikema JW. Scanning Hall Probe Microscopy of Magnetic Vortices in Very Underdoped yttrium-barium-copper-oxide. PhD thesis, 2004.
[55] Ge J, Gutierrez J, Cuppens J, Moshchalkov VV. Observation of single flux quantum vortices in the intermediate state of a type-I superconducting film. Phys. Rev. B, 88(17):174503, 2013.
[56] Ge J, Gutierrez J, Raes B, Cuppens J, Moshchalkov VV. Flux pattern transitions in the intermediate state of a type-I superconductor driven by an ac field. New J. Phys., 15(3):033013, 2013.
[57] Baert M, Metlushko VV, Jonckheere R, Moshchalkov VV, Bruynseraede Y. Composite Flux-Line Lattices Stabilized in Superconducting Films by a Regular Array of Artificial Defects. Phys. Rev. Lett. 74:3269–3272, 1995.
[58] Moshchalkov VV, Baert M, Metlushko VV, Rosseel E, Van Bael MJ, Temst K, Bruynseraede Y, Jonckheere R. Pinning by an antidot lattice: The problem of the optimum antidot size. Phys. Rev. B 57:3615–3622, 1998.
[59] Auslaender OM, Luan L, Straver EWJ, Hoffman JE, Koshnick NC, Zeldov E, Bonn DA, Liang R, Hardy WN, Moler KA. Mechanics of individual isolated vortices in a cuprate superconductor. Nature Phys., 5(1):35–39, 2009.
[60] Kalisky B, Kirtley JR, Analytis JG, Chu J-H, Fisher IR, Moler KA. Behavior of vortices near twin boundaries in underdoped $Ba(Fe_{1-x}Co_x)_2As_2$. Phys. Rev. B 83:064511, 2011.
[61] Raes B, Van de Vondel J, Silhanek AV, de Souza Silva CC, Gutierrez J, Kramer RBG, Moshchalkov VV. Local mapping of dissipative vortex motion. Phys. Rev. B 86:064522, 2012.
[62] Kramer RBG, Silhanek AV, Van de Vondel J, Raes B, Moshchalkov VV. Symmetry-Induced Giant Vortex State in a Superconducting Pb Film with a Fivefold Penrose Array of Magnetic Pinning Centers. Phys. Rev. Lett. 103:067007, 2009.
[63] Kramer RBG, Ataklti GW, Moshchalkov VV, Silhanek AV. Direct visualization of the Campbell regime in superconducting stripes. Phys. Rev. B 81:144508, 2010.
[64] Huebener R. Magnetic flux structures in superconductors: extended reprint of a classic text, volume 6. 2001.
[65] Valenzuela SO. Order and Mobility of Solid Vortex Matter in Oscillatory Driving Currents. Phys. Rev. Lett. 88:247003, 2002.

[66] Moshchalkov VV, Baert M, Metlushko VV, Rosseel E, Van Bael MJ, Temst K, Jonckheere R, Bruynseraede Y. Magnetization of multiple-quanta vortex lattices. Phys. Rev. B 54:7385–7393, 1996.
[67] Lefebvre J, Hilke M, Altounian Z. Strengthening of Reentrant Pinning by Collective Interactions in the Peak Effect. Phys. Rev. Lett. 102:257002, 2009.
[68] Ge J, Gutierrez J, Cuppens J, Moshchalkov VV. Quantification of the flux tubes and the stability of stripe pattern in the intermediate state of a type-1 superconducting film. Physica C 503:38–41, 2014.
[69] Hoberg JR, Prozorov R. Current-driven transformations of the intermediate-state patterns in type-I superconductors. Phys. Rev. B 78:104511, 2008.
[70] Avraham N, Khaykovich B, Myasoedov Y, Rappaport M, Shtrikman H, Feldman DE, Tamegai T, Kes PH, Li M, Konczykowski M et al. 'Inverse' melting of a vortex lattice. Nature, 411(6836):451–454, 2001.
[71] Sluchanko N, Gavrilkin S, Mitsen K, Kuznetsov A, Sannikov I, Glushkov V, Demishev S, Azarevich A, Bogach A, Lyashenko A et al. Superconductivity in ZrB_{12} and LuB_{12} with Various Boron Isotopes. J. Sup. Novel Mag., 26(5):1663–1667, 2013.
[72] Ge J-Y, Gutierrez J, Lyashchenko A, Filipov V, Li J, Moshchalkov VV. Direct visualization of vortex pattern transition in ZrB_{12} with Ginzburg–Landau parameter close to the dual point. Phys. Rev. B, 90(18):184511, 2014.
[73] Desorbo W. The Peak Effect in Substitutional and Interstitial Solid Solutions of High-Field Superconductors. Rev. Mod. Phys. 36:90–94, 1964.
[74] Weber HW, Seidl E, Botlo M, Laa C, Mayerhofer E, Sauerzopf FM, Schalk RM, Wiesinger HP, Rammer J. Magnetization of low-κ superconductors I the phase transition at H_{c1}. Physica C, 161(3):272–286, 1989.
[75] Muhlbauer S, Pfleiderer C, Boni P, Laver M, Forgan EM, Fort D, Keiderling U, Behr G. Morphology of the Superconducting Vortex Lattice in Ultrapure Niobium. Phys. Rev. Lett. 102:136408, 2009.
[76] Guillamon I, Suderow H, Fernandez-Pacheco A, Sese J, Cordoba R, De Teresa JM, Ibarra MR, Vieira S. Direct observation of melting in a two-dimensional superconducting vortex lattice. Nature Phys., 5(9):651–655, 2009.
[77] Babaev E, Ashcroft NW. Violation of the London law and Onsager–Feynman quantization in multicomponent superconductors. Nature Phys., 3(8):530–533, 2007.